Journal of Structural Biology 217 (2025) 108230

Contents lists available at ScienceDirect

Journal of Structural Biology

journal homepage: www.elsevier.com/locate/yjsbi

Research Article

Crystal structure, enzymatic and thermodynamic properties of the *Thermus thermophilus* phage Tt72 lytic endopeptidase with unique structural signatures of thermal adaptation

Sebastian Dorawa [a,1], Katarzyna Biniek-Antosiak [b,1], Magdalena Bejger [b], Anna-Karina Kaczorowska [c], Karol Ciuchcinski [d], Agnieszka Godlewska [a], Magdalena Płotka [c], Gudmundur O. Hreggvidsson [e,f], Lukasz Dziewit [d], Tadeusz Kaczorowski [a,*], Wojciech Rypniewski [b,*]

[a] *Laboratory of Extremophiles Biology, Department of Microbiology, Faculty of Biology, University of Gdansk, 80-308 Gdańsk, Poland*
[b] *Institute of Bioorganic Chemistry, Polish Academy of Sciences, Noskowskiego 12-14, 61-704 Poznań, Poland*
[c] *Collection of Plasmids and Microorganisms, Department of Microbiology, Faculty of Biology, University of Gdansk, 80-308 Gdańsk, Poland*
[d] *Department of Environmental Microbiology and Biotechnology, Institute of Microbiology, Faculty of Biology, University of Warsaw, Miecznikowa 1, 02-096 Warsaw, Poland*
[e] *Matis, Reykjavik, Iceland*
[f] *Faculty of Life and Environmental Sciences, University of Iceland, Reykjavik, Iceland*

ARTICLE INFO

Keywords:
Bacteriophage
Endolysin
Thermostable lytic protein
Crystal structure
M23 domain

ABSTRACT

We presents the discovery and molecular characterization of a novel lytic enzyme from the extremophilic *Thermus thermophilus* MAT72 phage vB_Tt72. The protein of 346-aa (MW = 39,705) functions as phage vB_Tt72 endolysin and shows low sequence identity (<37 %) to members of M23 family of peptidoglycan hydrolases, except for two uncharacterized endopeptidases of *T. thermophilus* phages: φYS40 (87 %) and φTMA (88 %). The enzyme exhibits lytic activity mainly against bacteria of the genus *Thermus* and, to a lesser extent, against other Gram-negative and Gram-positive bacteria. The protein is monomeric in solution and is highly thermostable (T_m = 98.3 °C). It retains ~ 50 % of its lytic activity after 90 min of incubation at 99 °C. Crystallographic analysis, at 2.2 Å resolution, revealed a fold characteristic of M23 metallopeptidases, accounting for 40 % of the structure. The remaining parts of the molecule are folded in a manner that was previously undescribed. The M23 fold contains a Zn^{2+} ion coordinated by a conserved His-Asp-His triad, and two conserved His residues essential for catalysis. The active site is occupied by a phosphate or a sulfate anion, while the substrate-binding groove contains a ligand, which is a fragment of *E. coli* peptidoglycan. The common sequence-based criteria failed to identify the protein as (hyper)thermophilic. It is likely that the protein's thermal stability is owed to peculiar features of its three-dimensional structure. Instead of trimmed surface loops, observed in many thermostable proteins, the catalytic domain contains two long loops that interlace and form an α-helical bundle with its own hydrophobic core.

1. Introduction

Phage lytic enzymes (endolysins) are synthesized during the latent phase of the phage lytic cycle. They target and degrade peptidoglycan (PG), the rigid layer of the cell wall, to release viral progeny (Loessner, 2005; Young, 2014; Abdelrahman et al., 2021). PG is an essential component of the bacterial cell wall that maintains cell shape and integrity. It is considered one of the most complex biological macromolecules, with a mesh-like structure consisting of linear glycan chains covalently interconnected by short stem peptides. Each glycan chain comprises alternating N-acetylglucosamine (GlcNAc) and N-acetylmuramic acid (MurNAc) disaccharide units linked by β-1,4-glycosidic bonds.

* Corresponding authors.
E-mail addresses: tadeusz.kaczorowski@ug.edu.pl (T. Kaczorowski), wojtekr@ibch.poznan.pl (W. Rypniewski).
[1] These authors contributed equally to this work.

https://doi.org/10.1016/j.jsb.2025.108230
Received 9 May 2025; Received in revised form 24 June 2025; Accepted 25 June 2025
Available online 26 June 2025

The short-stem pentapeptides that cross-link the glycan chains are attached by an amide bond to the D-lactyl moiety of the MurNAc. After processing by specific D-alanyl-D-alanine carboxypeptidase, these neighboring peptides may be interconnected via a direct transpeptide bond or a transpeptide bridge to form a sacculus-like structure surrounding the cell membrane (Vollmer et al., 2008a). This cross-linking strengthens the PG layer, enabling it to withstand the high internal turgor pressure generated by the cytosolic compartment.

In the extreme thermophilic Gram-negative eubacterium *Thermus thermophilus*, the basic monomeric unit of PG is composed of GlcNAc-MurNAc-L-Ala^1-D-γ-Glu^2-L-Orn^3-D-Ala^4-D-Ala^5 muropeptide. It is acylated at the δ-amino group of ornithine via a diglycyl transpeptide, which cross-links neighboring stem peptides through residues at positions 3 and 4, respectively (Quintela et al., 1995). This structure corresponds to the rare A3β PG chemotype, also found in *Deinococcus radiodurans* (Quintela et al., 1999a). While common in Gram-positive bacteria (e.g., *Staphylococcus aureus*), the oligoglycine-mediated interconnection between stem peptides is exceptional among Gram-negative microbes (Quintela et al., 1995; Kim et al., 2015). It has also been shown that the glycyl residues in *T. thermophilus* PG not involved in bridge formation are acylated with phenylacetic acid (Quintela et al., 1995; Quintela et al., 1999b). This unique modification, found in 23.7 % of total muropeptides, effectively blocks transpeptidation acceptor sites and leads to lower glycan chain cross-linkage (Quintela et al., 1995; Vollmer et al., 2008b). It is further postulated that PG decoration with aromatic moieties facilitates interactions with hydrophobic regions of other *T. thermophilus* cell wall components (Quintela et al., 1995; Acosta et al., 2012a; Acosta et al., 2012b).

The complexity of PG is matched by the diversity of lytic enzymes involved in its degradation. Based on substrate specificity, lysins are divided into three types: (i) endopeptidases targeting peptide bonds (e.g. L-alanoyl-D-glutamate endopeptidases and interpeptide bridge endopeptidases), (ii) amidases targeting amide bonds (e.g. *N*-acetylmuramoyl-L-alanine amidases) and (iii) glycosidases targeting glycosidic bonds (e.g. *N*-acetyl-β-D-glucosaminidases, *N*-acetyl-β-D-muramidases, and transglycosylases) (Vollmer et al., 2008b; Oliveira et al., 2018). The specificity of endolysins for PG makes them promising candidates as antimicrobials. This provides a strategy for developing novel therapeutics that selectively eliminate pathogenic bacteria while minimizing resistance development (Dams and Briers, 2019). In this regard, lysins from thermophilic phages are particularly noteworthy (Aevarsson et al., 2021). Recently, we discovered and characterized three novel endolysins from *T. scotoductus* phages Ph2119 (Plotka et al., 2014) and Tsc2631 (Plotka et al., 2015), and from *T. thermophilus* phage phiKo (Szadkowska et al., 2024). All three lysins are highly thermostable but unexpectedly show no sequence similarity to known thermophilic phage lytic enzymes. Instead, each harbors a catalytic site with three conserved residues forming a Zn^{2+} binding site, characteristic of T3 and T7 lysozymes and eukaryotic peptidoglycan recognition proteins—key components of innate immunity from insects to mammals (Dziarski and Gupta, 2010; Royet et al., 2011).

In silico analysis and crystal structure insights enabled us to identify and characterize the AMI-2-type catalytic domain in each case (Plotka et al., 2019b; Plotka et al., 2020). This domain is typical of *N*-acetylmuramoyl-L-alanine amidases that cleave the amide bond between the *N*-acetylmuramoyl residue and the L-Ala of the stem peptide (Plotka et al., 2019b; Plotka et al., 2020). The thermostability of these enzymes led us to assess Tsc2631 endolysin as a potential antimicrobial agent against multidrug-resistant strains of *Acinetobacter baumannii* and *Pseudomonas aeruginosa*, members of the ESKAPE group posing serious public health threats (De Oliveira et al., 2020). Antibacterial tests showed a 1.4–3.7 log reduction in bacterial load, with the killing effect enhanced by outer membrane permeabilizers such as EDTA (0.5 mM) and, to a lesser extent, malic acid (0.6 mM) and citric acid (0.4 mM) (Plotka et al., 2019a).

This study aimed to structurally and functionally characterize the endopeptidase LysTt72 from *T. thermophilus* MAT72 phage. This enzyme shows low amino acid sequence similarity to members of the M23 peptidase family, a group of PG hydrolases that typically cleave the glycyl bonds within stem peptide cross-bridges (Razew et al., 2022). To our knowledge, this is the first molecular-level report of a thermostable M23-type metallopeptidase from a thermophilic phage. The protein displays unique structural features that likely contribute to its thermostability.

2. Results

2.1. In silico analysis of the T. thermophilus phage vB_Tt72 genome in search of lytic enzymes

A BLASTP analysis of the Tt72 phage genome (~154 kb) revealed an open reading frame with an amino acid sequence similar to members of the M23 metallopeptidase family (Pfam: PF01551), which primarily target bacterial peptidoglycan. The corresponding nucleotide sequence was deposited in GenBank (accession number PQ465150). The *lysTt72* gene comprises 1041 nucleotides and encodes a 346-amino acid (aa) protein with a predicted molecular weight of 39,705 Da and an isoelectric point of 8.9. The gene starts with the initiation codon ATG and ends with the TAA termination codon. Its overall guanine-plus-cytosine (G + C) content is 31.1 %, which is much lower than the G + C content of *T. thermophilus* genomic DNA (69.5 %) (Henne et al., 2004). The codon usage of the *lysTt72* gene reflects this low G + C content, with 80.9 % of the codons ending in A or T. To assess the codon usage differences between *lysTt72* and the *T. thermophilus* genome, we calculated the codon adaptation index (CAI) using the JCat tool (Grote et al., 2005). Given that genes with high CAI values (near 1) are typically expressed efficiently, the CAI of 0.65 for *lysTt72,* suggests a moderate rate of expression in the host bacterium.

To explore the evolutionary relationships between LysTt72 and other viral M23 peptidases, a phylogenetic analysis was conducted. First, 1512 viral protein sequences containing the PF01551 domain were retrieved from UniProt. Proteins with additional Pfam domains were excluded, yielding a final dataset of 417 sequences containing only the M23 domain. To reduce redundancy, the sequences were clustered at 70 % coverage and identity, resulting in 153 clusters. Representative sequences from each cluster were used for maximum-likelihood phylogenetic tree construction. Bacterial M23 peptidases were included as an outgroup.

The primary outcome of the phylogenetic analysis was the host distribution pattern, depicted in the outer circle of the tree, where a clear pattern of host specificity among the viral M23 peptidases emerged (Fig. 1a). Most peptidases originated from bacteriophages infecting genera such as *Arthrobacter* (clusters 1–2), *Thermus* (cluster 3), *Bacillus* (cluster 4), *Staphylococcus* (cluster 5) and *Curtobacterium* (cluster 6). Notably, most clusters exhibited host-genus specificity, suggesting potential co-evolution between viral peptidases and their bacterial hosts. Finally, a clear distinction can be seen between peptidases from *Thermus* phages and the rest of the tree, further underlining the unique properties of LysTt72 peptidase. Additionally, the structure-guided tree was prepared using structures for all sequences included in the phylogenetic tree predicted with AlphaFold3 and then aligned using FoldMason. In general, most of the clusters visible in the phylogenetic tree can be seen in the structure-guided tree, with the exception of cluster 3, which contains peptidases originating from *Thermus* phages, that are scattered over the tree, and do not form a cluster. However, it must be noted that the quality of obtained structures (mean pLDDT <80) was questionable. Therefore, any obtained result must be interpreted with caution, since it cannot be determined whether this result stems from actual data or prediction errors. As such, we have included the tree as a supplementary figure (Fig. S1).

LysTt72 shares low identity with well-characterized M23 metallopeptidases such as LytM from *S. aureus* (GenBank WP_000736792.1;

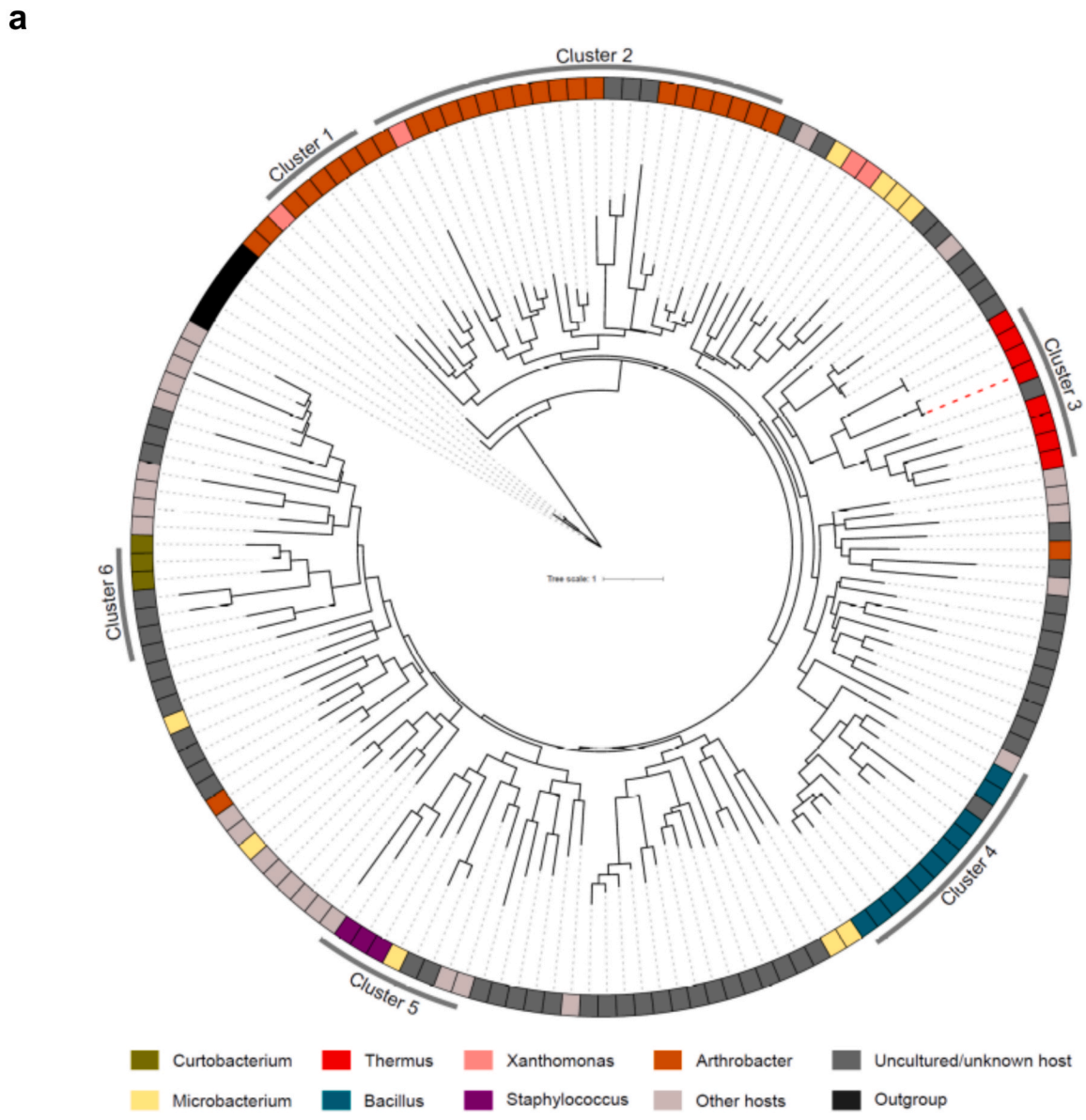

b

```
LysTt72      114-FHPGVDINYGS--ENQDFGLPVYAVTDGVVIMASRHFCSASCDCSG--FVAVEHRCQN-----------KIFYALYGHVVP-EANICKKVKAGERIASIGEYKC--NSTSHLHLE-210
LysP74-26_   11-PHPGYDLNFGP-TPDADYGQAVYAPEDGKVVFAKQ----GLGTWGG--LVVVLGASG-----------YAHRLGHVERMTVKEGQRVKEGDQVAVIGRVQG----MAPHLHYD-101
LysP23-45_   23-PHPGYDLNFGP-TPDADYGQAVYAPEDGKVVFARQ----GLGTWGG--LVVVLGASG-----------YAHRLGHVERMTVKEGQQVKEGDQVAVIGRVQG----MAPHLHYD-113
Lys_Siphov   36-YHPGWDLNFG--SGNDQCGLDVSAMADGIVNYSGG----PSKGWGN--HVVIFHP----QYNV---------YSHYAHLKEFSVKKGEDVRRGQVFAHVGKTG---TKYCHVHFE-126
LysIN93      49-WHTGVDLNGPG-GGDTDCGQPVHAMTDGRVVIAG-----RFPVWGG--MVVLWHP----SAGV---------WTRYGHLRDILVHPGDVVVAGQQIGTIGKMT--TGGYCHLHFD-140
LysphiMa     34-PHTGEDWNLRT-GGDSDLGYPVQAVFPGTVVAAG-----WYRVWGN--LVVVRVDPWVQELLQKALGEPLEDLYVRYGHLHHTVVTQGQQVDAGECIGSIGKGDG-GRYMAHLHID-140
MMPphg       37-AEHTGVDYNLVGTSGDADLGYPVVAMADGIVRHAR-----AHRIWGN--IVLLEHP----QLGL---------WSQYAHLYQLAVDAGQEIWAGEPLGSIGRGDPRAPFLAHLHFE-131
Lys_phiLo_   38-EHPGVDINIHGTSGNQDFGWPVVSIGEGVVVHVG-----SHRVWGK--IVLIHHPTFKKLLGLDHE------VYSQYAHLHQVCVSDGDYVYPGYPVGSIGNGDPLKPFLAHLHFE-141
LysTMA       114-FHPGVDINYGS--GNQDLGLPVYAVTDGIVIMASRRFCSASCDCSG--FVAIEHRCQD-----------KVFYALYGHVVP-EVNICKKVKAGERIASIGEYKC--NSTSHLHFE-210
LysYS40      114-FHPGVDINYGS--GNQDLGLPVYAVTDGVVIMASRQFCSASCDCSG--FVAIEHRCQN-----------KIFYALYGHVVP-EVSICKKVKAGERIALIGEYKC--NSTSHLHFE-211
LytM         209-AHYGVDYAMPE-------NSPVYSLTDGTVVQAG------WSNYGGGNQVIIKEANSN-----------NYQWYMHNNRLTVSAGDKVKAGDQIAYSGSTGN--STAPHVHFQ-295
```

Fig. 1. Phylogenetic analysis and multiple sequence alignment of M23 peptidases. (a) Phylogenetic tree depicting the evolutionary relationships between phage M23 peptidases. The LysTt72 peptidase is marked with a red dashed line. The outer circle indicates the bacterial host for each virus. (b) Multiple sequence alignment of LysTt72 and selected M23 peptidases. The alignment was performed using CLUSTAL W (Thompson et al., 1994). The GenBank accession numbers of lysins used in the comparative analysis are as follows: PQ465150 (LysTt72), YP_001468077.1 (LysP74-26), YP_001467961.1 (LysP23-45), QGH73463.1 (Lys_Siphoviridae), NP_777327.1 (LysIN93), WP_126178192.1 (LysphiMa), QAY18044.1 (MMPphg), AYJ73924.1 (Lys_phiLo), YP_004782349.1(LysTMA), YP_874157.1 (LysYS40), and WP_000736792.1 (LytM). Conserved residues coordinating Zn^{2+} cation are marked with red triangles, while black triangles indicate residues responsible for activating a water molecule to function as a nucleophile. (For interpretation of the references to colour in this figure legend, the reader is referred to the web version of this article.)

27 % identity, 47 % query coverage), lysostaphin (Lss) from *S. simulans* (AAB53783.1; 24 % identity, 41 % query coverage), and MMPphg from *Meiothermus* phage MMP17 (QAY18044.1; 31 % identity, 32 % query coverage). On the other hand, LysTt72 shows a high level of identity with two yet uncharacterized M23-type peptidases of *T. thermophilus* phages: φYS40 (GenBank: YP_874157.1; 87 % identity, 100 % query coverage) and phage φTMA (YP_004782349.1; 88 % identity, 100 % query coverage) isolated from hot springs in Japan (Naryshkina et al., 2006; Tamakoshi et al., 2011). Both of them, as well as Tt72 phage, belong to myoviruses. Another match for the LysTt72 sequence was found with a 92-amino acid fragment (GenBank: MEM0333274.1) attributed to *Candidatus Aenigmatarchaeota* archaeon identified in a metagenomic project (Qi et al., 2024). The sequence is almost identical with the N-terminal part of LysTt72 (single difference: Asn vs. Asp), which could indicate that it is in fact a fragment of the *T. thermophilus* vB_Tt72 phage genome or a closely related one.

Enzymes of the M23 peptidase family target the glycyl bonds within oligoglycine cross-bridges that interconnect stem peptides (Razew et al., 2022). According to the Conserved Protein Domain Family classification (Wang et al., 2023), LysTt72 possesses a single enzymatically active domain (M23_peptidase, accession: cd12797) with a conserved catalytic motif: **H**(x)$_n$**D** and Hx**H** (Rawlings et al., 2004). As in other M23 peptidases (e.g. LytM, (Grabowska et al., 2015), the conserved residues His115, Asp119 and His208 coordinate a Zn^{2+} ion. Additionally, His176 and His206 activate a water molecule for nucleophilic attack (Fig. 1b).

2.2. Characterization of LysTt72 lytic activity

The lytic activity of the purified recombinant LysTt72 (Fig. S2 and S3) was determined under different conditions via a turbidity reduction assay using chloroform-treated *T. thermophilus* MAT72 cells as a substrate (Fig. 2). The activity increased proportionally to the LysTt72 enzyme concentration until saturation was reached at 50 μg/mL of protein after 60 min of the assay (Fig. 2a). The effect of temperature was tested in the range of 20–90 °C. LysTt72 was active over a wide range of temperatures, and the highest activity was observed at 50 °C (Fig. 2b). This finding is surprising, considering that the optimal temperature for *T. thermophilus* MAT72 growth is 65–72 °C, with minimal and maximal temperatures of 47 and 85 °C, respectively (Oshima and Imahori, 1974). Analysis of the effect of pH from 5.0 to 11.0 revealed that the optimum pH was 9.5 (Fig. 2c), which matches the enzyme's isoelectric point of 8.9 and suggests that the LysTt72 requires a negative net charge for full activity. Regarding ionic strength, LysTt72 showed the highest activity at low KCl concentration (25 mM) (Fig. 2d).

2.3. Thermal stability of LysTt72

First, we investigated thermophilic indices related to the amino acid content of LysTt72. The EK/QH ratio (r_i index, (Farias and Bonato, 2003) for this enzyme was calculated to be 1.90, which corresponds to proteins from mesophiles ($r_i < 2.5$) rather than thermophiles ($3.2 < r_i <$

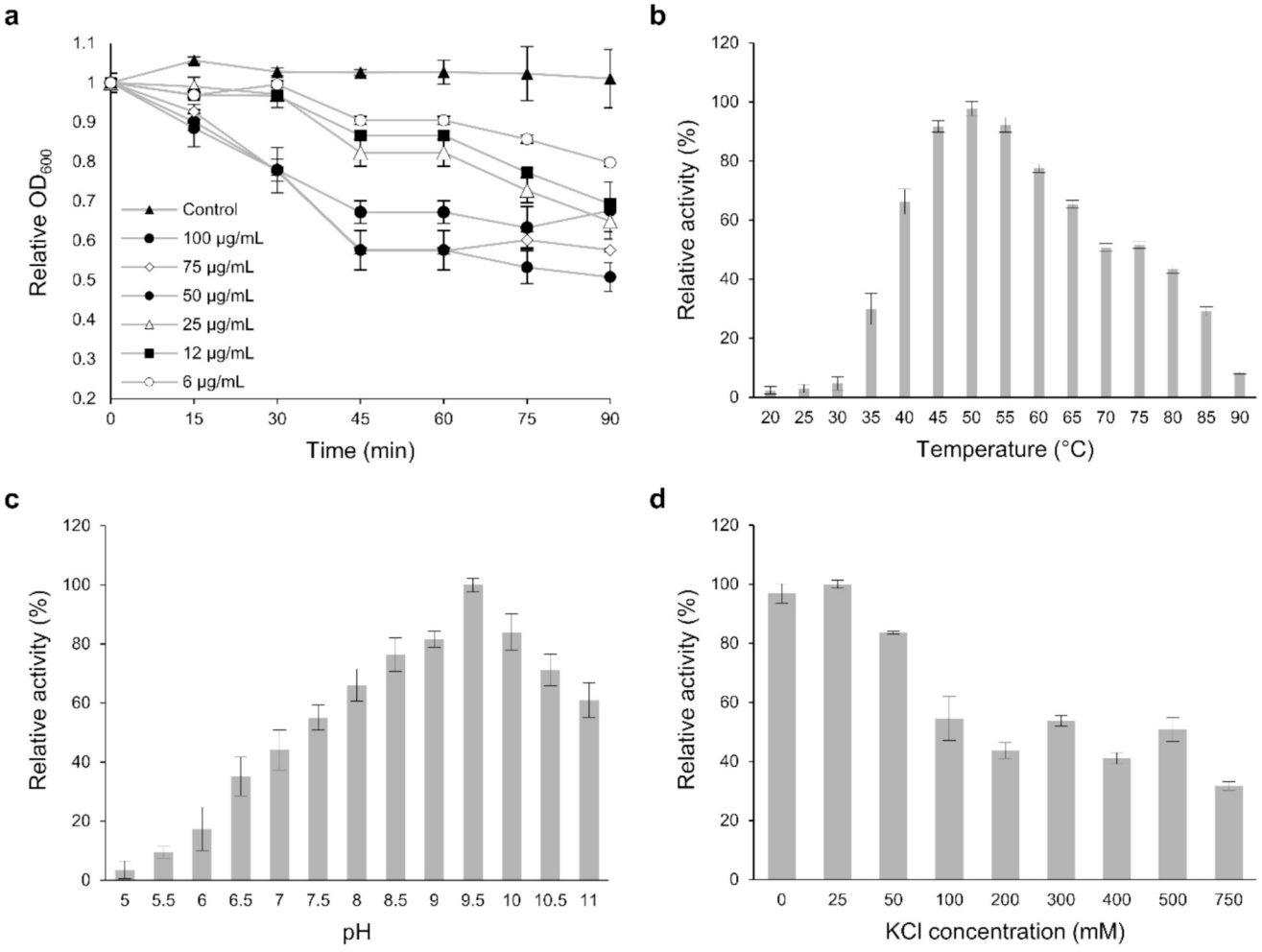

Fig. 2. Lytic activity of LysTt72 at different experimental settings. (**a**) The effect of different concentrations of recombinant LysTt72, (**b**) the effect of temperature, (**c**) the effect of pH, and (**d**) the effect of KCl concentration. The enzyme lytic activity was measured using a turbidity reduction assay and chloroform-treated *T. thermophilus* MAT72 cells as a substrate. The relative activity against *T. thermophilus* MAT72 cells was calculated by comparing the lytic activity at specific conditions with the maximal lytic activity among the datasets. Each experiment was repeated in triplicate; error bars indicate the standard deviation.

4.5) or hyperthermophiles ($r_i > 4.5$). Generally, in highly thermostable proteins, this parameter indicates a strong preference for Glu, Lys, Tyr, and Ile over Gln, His, Ala, and Cys, with a high content of the latter noted in proteins from mesophilic sources. Secondly, the value of the CvP bias parameter (charged versus polar amino acids (Suhre and Claverie, 2003) of –10.4 differs substantially from proteins with high thermal stability (CvP > 7.4), as they show a strong bias for charged residues over polar residues (Ma et al., 2006). This parameter discriminates against thermophilic proteins and is often used in bioinformatics analyses (Taylor and Vaisman, 2010). In the case of LysTt72, we observe a peculiar prevalence of polar over charged residues. The IVYWREL index (Zeldovich et al., 2007) of 0.36 is also lower than expected for a thermophilic protein. The aliphatic index of LysTt72, which is another measure used in assessing thermostability, equals 76.7, closer to the average value for mesophilic (78.8) rather than thermophilic (92.6) proteins (Ikai, 1980). When the amino acid composition of LysTt72 is compared with values of the average amino acid content, derived from a large collection of proteins (Carugo, 2008), the largest deviations are observed for Asn, of which LysTt72 contains 33, amounting to 9.5 % of its amino acid content, compared to the overall average of 3.9 %; Tyr residues (28, 8.1 % vs. 2.9 %), and Trp (only one in LysTt72, 0.3 % vs. 5.3 %). It is not clear how these deviations could be related to the thermostability of LysTt72.

In laboratory settings, the thermal resistance of LysTt72 was determined by heating protein samples to 99 °C, followed by measurement of the enzyme's residual lytic activity with a standard turbidity reduction assay. LysTt72 retained 51 % of its initial activity after 90 min at 99 °C (Fig. 3a). The protein's thermal stability was precisely determined by nanoscale differential scanning fluorimetry (nanoDSF) and back-reflection technology. The calculated inflection temperature of the thermal unfolding of LysTt72 was 98.3 ± 0.5 °C (Fig. 3b). The recombinant enzyme demonstrated fold stability up to approximately 82 °C (Fig. 3b). Additionally, a well-defined unfolding transition was observed between 70 and 100 °C, leading to irreversible denaturation. The LysTt72 onset temperature aggregation and temperature mid-aggregation were 64.9 ± 1.0 °C and 93.0 ± 1.0 °C, respectively (Fig. 3b). This analysis confirmed the enzyme's high thermal stability.

2.4. Substrate specificity

The substrate specificity of LysTt72 was tested against both mesophilic and thermophilic chloroform-treated bacteria. As expected, the highest lytic activity was observed against bacteria of the genus *Thermus*

Table 1
LysTt72 substrate specificity. The relative activities are expressed as the percentage of *T. thermophilus* MAT72 activity. The values represent the means ± standard deviations ($n = 3$).

Organisms	Relative lytic activity (%)
Thermus thermophilus MAT72	100.0 ± 5.5
Thermus flavus MAT1087	89.1 ± 5.6
Thermus parvatiensis DSM 21745	109.1 ± 6.1
Thermus thermophilus HB8 DSM 579	78.9 ± 4.1
Thermus thermophilus HB27 DSM 7039	80.5 ± 3.5
Thermus scotoductus MAT2631	77.4 ± 5.0
Acinetobacter baumannii KPD 205-BA	12.6 ± 0.9
Bacillus megaterium ATCC 14581	0
Bacillus subtilis KPD 10	0
Deinococcus radiodurans ATCC 13939	16.3 ± 5.8
Escherichia coli MG1655 KPD 26-BA	8.5 ± 1.6
Listeria monocytogenes KPD 1326	0
Pseudomonas aeruginosa KPD 124	17.6 ± 9.5
Salmonella enterica serovar *Panama* KPD 101-BA	28.2 ± 2.1
Serratia marcescens KPD 102-BA	1.7 ± 0.5
Staphylococcus aureus KPD 19	6.7 ± 1.5

(Table 1). Notably, the enzyme showed greater activity against the *T. parvatiensis* DSM 21745 (109.1 ± 6.1 %) strain than against its native host, *T. thermophilus* MAT72 (100.0 ± 5.5 %). In contrast, LysTt72 displayed lower lytic activity against other *Thermus* strains compared to its activity against the native host strain. Additionally, LysTt72 demonstrated lytic activity against several mesophilic Gram-negative and Gram-positive bacteria, including *Salmonella enterica* serovar Panama KPD 101-BA (28.2 ± 2.1 %) and *S. aureus* KPD19 (6.7 ± 1.5 %). These results align with the general observation that globular endolysins derived from phages infecting Gram-negative bacteria tend to exhibit a broader substrate spectrum (Briers and Lavigne, 2015).

The effects of LysTt72 on the morphology of *T. thermophilus* MAT72 cells were analyzed using transmission electron microscopy (TEM). In the control experiment, the cell shape of the bacteria not treated with LysTt72 remained unaltered. Exposure of the bacteria to LysTt72 at a concentration of 100 μg/mL for 2 h at 55 °C did not cause significant changes in the cells' morphology (Fig. 4a). Most likely, the enzyme cannot penetrate the outer envelope of native *T. thermophilus* cells (Fig. 4b).

2.5. Overall structure of LysTt72

The crystallographic model of LysTt72 was built based on 2.2 Å

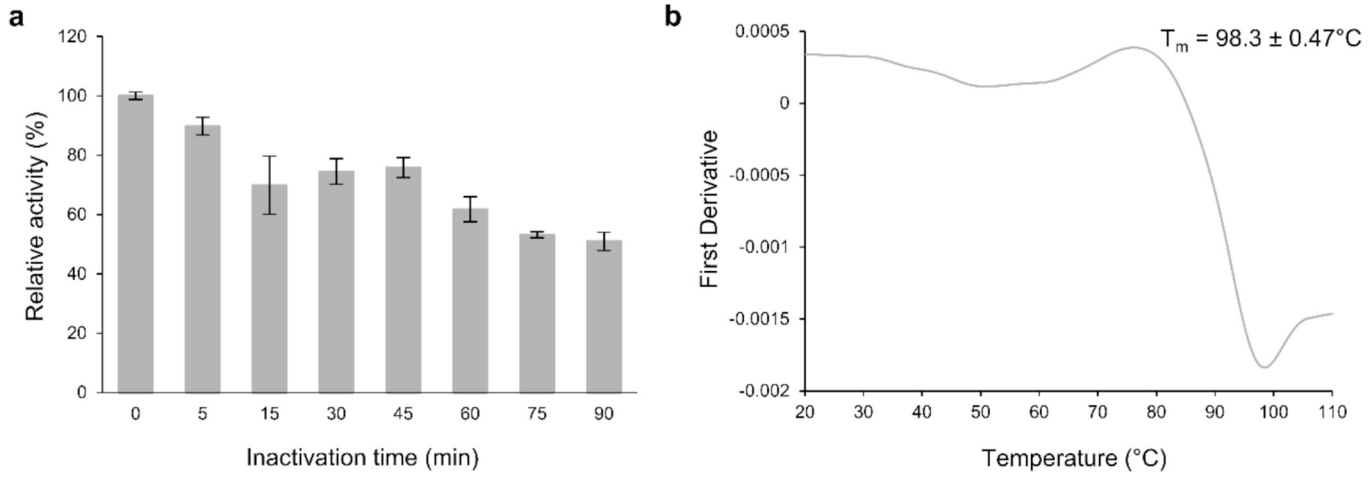

Fig. 3. Examination of the thermal stability of LysTt72. (**a**) The activity of LysTt72 after the enzyme was heated at 99 °C for 5–90 min compared to that of the untreated control. Each experiment was repeated in triplicate; the error bars indicate standard deviations. (**b**) Analysis of LysTt72 stability by nanoDSF. The Y-axis represents the first derivative of the fluorescence intensity ratio of 350/330 nm measured by nanoDSF. T_m value represents the mean of triplicate measurements, and the standard deviation is indicated.

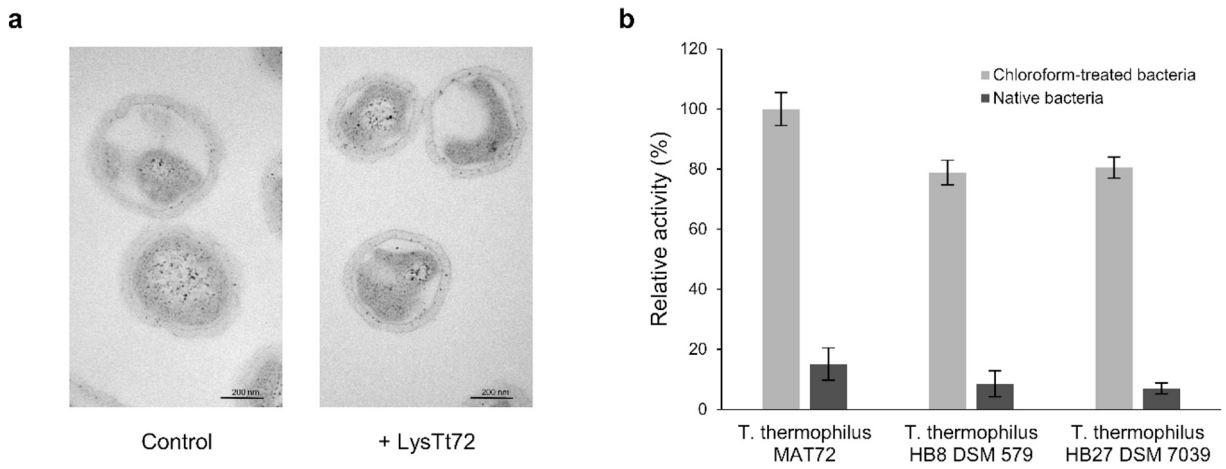

Fig. 4. Transmission electron microscopy analysis of *T. thermophilus* MAT72 cells treated with LysTt72. (**a**) Bacteria were incubated with LysTt72 at the concentration 100 μg/mL (55 °C, 2 h). The scale bar represents 200 nm. In the control experiment native bacteria not treated with LysTt72 were used. (**b**) Activity of LysTt72 against native and chloroform-treated *T. thermophilus* cells. Lytic activity was measured in a standard turbidity assay against chloroform-treated and intact *T. thermophilus* MAT72 bacteria. In each case, the enzyme's activity is expressed as a percentage of the maximal lytic activity of the LysTt72 against chloroform-treated *Thermus thermophilus* MAT72 cells. Error bars indicate the standard deviation ($n = 3$). For all tests, bacterial cells were treated with LysTt72 at a concentration of 50 μg/mL (60 °C, 60 min).

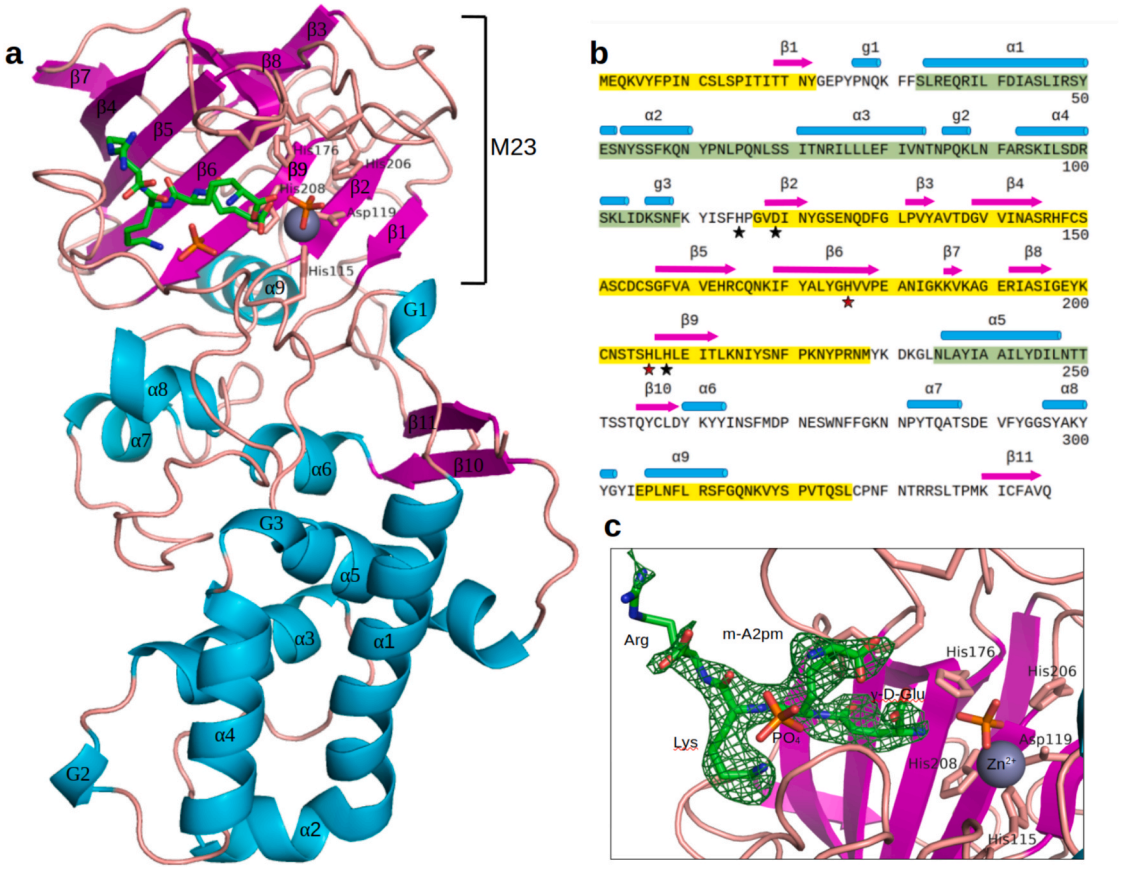

Fig. 5. (**a**) Cartoon drawing of the LysTt72 crystal structure, showing the β-sheets (*pink*), α-helices (*cyan*), bound peptide (colored sticks, green C-atoms), phosphate anions (sticks, orange), and Zn^{2+} (gray sphere). The conserved zinc-binding His115-Asp119-His208 triad and the two His residues essential for catalysis are shown (pink sticks) and labeled. The M23 catalytic domain is marked with a bracket. **(b)** The annotated amino acid sequence of LysTt72 shows the catalytic subdomain (yellow highlight), lower subdomain (green), and the middle region (no highlight). The secondary structures are labeled as in panel a: β-strands (arrows), α-helices (cylinders), the conserved His115-Asp119-His208 triad (black stars), coordinating the Zn^{2+} cation (gray sphere), and the two conserved His176 and His206 residues essential for catalysis (red stars). **(c)** The "omit" electron density (green mesh) for the peptidoglycan fragment bound in the LysTt72 substrate-binding site, identified as γ-D-Glu-m-A2pm-L-Lys-L-Arg from *E. coli* murein (see text). The map is contoured at 2.5 root-mean-square (r.m.s.) level.

resolution X-ray diffraction data by extending and refining a starting model, which contained 137 amino acid residues (Gln3-Tyr26, Ser113-Leu213 and Gly302-Phe313) selected from the AlphaFold model that superimposed closely with an experimentally determined structure of the M23 domain (see "Methods" section). Despite this cautious approach to the model predicted by AlphaFold2, it was noted eventually that almost the entire predicted model was remarkably accurate, including the parts of the structure for which no experimentally determined structures could be used as a guide (Fig. S4).

The final crystallographic model of LysTt72 is a monomer consisting of 346 amino acid residues. Size-exclusion chromatography confirmed that the enzyme exists as a monomer in solution (Fig. S3). The molecule appears to contain two distinct subdomains, with an intermediate zone also containing some well-defined secondary structure. This appearance of the protein being organized into domains is somewhat misleading because each subdomain is, in fact, a patchwork of different parts of the sequence, as the amino acid chain winds back and forth between them (Fig. 5a, b). The Peptidase_M23 enzymatic domain consists of three segments of the amino acid chain, separated in the sequence by two long insertions. The insertions are found only in LysTt72 and the two closely related phage peptidases, LysTMA and LysYS40 (Fig. 1b and Fig. S5). They loop out of the catalytic domain and fold into an α-helical bundle (α1–α5), other minor elements of the secondary structure and irregular loops. The two insertions, together with the last 20 residues at the C-terminus, account for most of the protein's bulk.

The main part of the M23 domain, which was identified by bioinformatic analysis of the LysTt72 sequence, consists of approximately 115 amino acids (residues 115–230) and corresponds to the middle part of the polypeptide chain. It includes β-strands β2–β9, containing a "Greek key" motif (strands β5 and β6 are rolled up extensions of β4 and β7). According to Pfam, the domain is classified as PF01551 (Peptidase_M23) and is characteristic of zinc-dependent endopeptidases (Razew et al., 2022). In addition to the main part, the catalytic subdomain includes two other segments of the amino acid chain: 22 residues at the N-terminus (residues 1–22), containing strand β1, and a similar-sized stretch (residues 305–326) near the C-terminus, containing helix α9. Together, the three segments of the amino acid chain form a well-ordered extended β-sheet (strands β1–β9), an α-helix and some irregular coils.

The α-helical bundle at the other end of the molecule consists of five α-helices, four of which (α1–α4) are formed by the first insertion extending out of the catalytic domain, between the β-strands β1 and β2, while the fifth helix, α5, is part of the second insertion in the catalytic domain. Helix α5 has a predominantly hydrophobic character, containing nine hydrophobic residues (Leu236, Ala237, Ile239, Ala240, Ala241, Ile242, Leu243, Ile246, Leu247), two tyrosines (Tyr238, Tyr244) which also have a partly hydrophobic character, due to their aromatic rings; and only one hydrophilic residue, Asp245. The helix is anchored between helices α1, α3, α4, α6 and strand β10.

The middle part of the LysTt72 molecule consists of three short α-helices (α6, α7 and α8) with an irregular coil in between and a pair of β-strands (β10 and β11). The molecule is stabilized by four disulfide bridges: Cys11–Cys327, Cys149–Cys155, Cys153–Cys201 and Cys257–Cys342. The first and last bridges are close to the N- and C-termini of the polypeptide chain, anchoring them to the bulk of the protein, while the middle two bridges link loops between strands β4 and

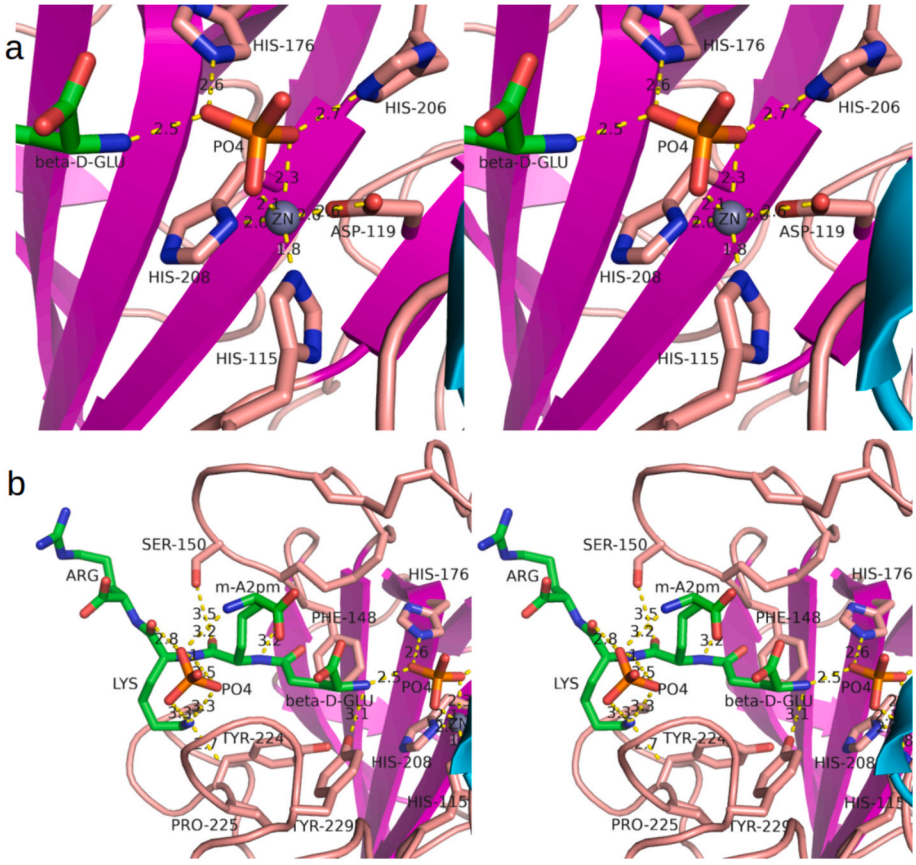

Fig. 6. Stereo view of the LysTt72 (**a**) active site showing the Zn^{2+} cation (gray sphere, drawn for clarity at 50 % ionic radius) held in place by the conserved triad of His115-Asp119-His208 residues, the phosphate (PO_4) anion bound to the cation in a bidentate manner; this structure is stabilized by the two conserved His176 and His206, considered to be essential for catalysis. Part of the bound peptidoglycan (see below) is also shown (γ-D-Glu, on the left). (**b**) The substrate-binding site with the bound ligand interpreted as γ-D-Glu-m-A2pm-L-Lys-L-Arg. Hydrogen bonds are drawn as yellow dotted lines, the distances are marked in Å. (For interpretation of the references to colour in this figure legend, the reader is referred to the web version of this article.)

β5 and between β8 and β9 that form one side of the substrate-binding groove near the active site.

Analysis performed on the DALI server (Holm, 2020) identified structural homologs among peptidases M23, overlapping only the catalytic subdomain, especially the β-sheet (Fig. S6). It seems that the rest of the LysTt72 fold has not been described before.

3. Substrate binding and the active site

The active site of LysTt72 is located in a distinct groove on the surface of the protein and is marked by a Zn^{2+} cation coordinated by a conserved His-Asp-His trio of residues (His115, Asp119, His208) (Fig. 6a). The identity of the Zn^{2+} cation was confirmed by its fluorescence in an X-ray energy scan and by the presence of anomalous density peaks in all three examined crystal structures (peak heights: 6, 13 and 9 for the crystals LysTt72, LysTt72a and LysTt72b, respectively). Zn^{2+} coordination is completed by a phosphate or sulfate anion (both were present in the crystallization solution). Two of its oxygen atoms complete the coordination sphere around Zn^{2+}. In addition, the oxygen atoms of the anion interact at H-bonding distances with the N^{ε} atoms of His176 and His206, the hydroxyl O atoms of Tyr26 and Tyr199, and a water molecule.

Further along the substrate-binding groove, unexpected electron density was observed (Fig. 5c) and interpreted as a fragment of the *E. coli*'s peptidoglycan (γ-D-Glu with *meso*-diaminopimelic acid (m-A2pm)) attached to a terminal fragment of Braun's lipoprotein (L-Lys-L-Arg) (Vollmer and Bertsche, 2008). The sequence γ-D-Glu-m-A2pm-L-Lys-L-Arg has the N-terminal group of γ-D-Glu close to the phosphate anion in the active center, while its carboxyl terminal group is disordered. Residues m-A2pm and Lys fit well into the electron density. The side chain of Lys is nestled in an electronegative cavity formed by three main chain carbonyl O atoms of Pro221, Tyr224 and Pro225 (Fig. 6b). Another phosphate (or sulfate) ion is adjacent to the bound peptide, and this ion makes three H-bonds with the peptide (with the NH_2 group of m-A2pm and with the main chain amino and carbonyl groups of Lys), one H-bond with the protein (main chain N of Asn227) and an ordered water molecule deep in the substrate binding groove. Electron density can be observed for the main chain of Arg, while the side chain protrudes out of the binding groove and is also disordered.

4. Discussion

In the midst of the antibiotic resistance crisis, phage lytic enzymes are gaining attention as promising antimicrobials with a targeted killing potential to combat bacterial pathogens in a highly specific manner (São-José et al., 2022). Of particular interest are the robust lysins encoded by thermophilic phages, which represent a compelling group within the category of bacterial cell-wall degrading enzymes (Plotka et al., 2014; Plotka et al., 2019b; Plotka et al., 2019a). Their high thermal resistance, compact structure, and broad-spectrum antimicrobial activity against both Gram-positive and Gram-negative bacteria make them excellent candidates for developing tailored anti-infectives. Such custom-engineered lysins, exemplified by the Artilysins produced through VersaTile-driven technology, have proven to be highly effective against the ESKAPE group of pathogens, the leading cause of nosocomial infections worldwide (Gerstmans et al., 2020; Zeng et al., 2024). LysTt72, the *T. thermophilus* phage Tt72 endolysin characterized in this report, belongs to the family of M23 lytic metallopeptidases, which specifically target peptide bonds within the bacterial cell wall peptidoglycan layer. Their primary specificity involves cleaving the glycyl bonds within stem peptide cross-bridges. These enzymes play a crucial role in bacterial cell wall remodeling and degradation, making them essential for processes such as cell division and bacterial cell lysis.

LysTt72 demonstrates remarkable thermal stability, with a melting temperature (T_m) of 98 °C. However, its amino acid composition does not display the typical features associated with thermophilic proteins. The values of discriminatory parameters such as the EK/QH ratio, CvP bias, IVYWREL index, and aliphatic index differ substantially from those expected of proteins of thermophilic origin. Were it not for the biophysical data, the sequence-based indicators would erroneously place LysTt72 in the mesophilic range. This raises a question about the basis of LysTt72′s thermal adaptation.

As the sequence-based analysis fails to account for the protein's thermostability, one should look for an explanation in the three-dimensional structure of the molecule. First, it is important to note the presence of disulfide bridges, which are often associated with thermostability. Indeed, four such bridges are present in LysTt72. Two of them (Cys11–Cys327 and Cys257–Cys342) are located near the N- and C-termini, anchoring them to the bulk of the molecule. The other two (Cys149–Cys155 and Cys153–Cys201) are situated near the active site, stabilizing the substrate-binding cavity.

Furthermore, the protein's stability is likely influenced by the way the polypeptide chain is folded. The structure of LysTt72 contrasts with earlier observations that many thermostable proteins have shorter surface loops, compared to their mesophilic analogues. Loop shortening has been viewed as a means to enhance structural stability by reducing potential fluctuations (Kumar et al., 2000). However, the evolution of LysTt72 appears to have taken the opposite direction. The loops extending from the catalytic domain are unusually long and fold into a well-defined, mostly α-helical structure with its hydrophobic core. The two extensions are interlaced, with helix α5 from the second extension wedged into the helical bundle formed by the first extension (Fig. 5a and b). This unusual pseudodomain, composed of two distinct parts of the amino acid sequence, is stabilized by hydrophobic interactions centered around the highly nonpolar helix α5 (Fig. S7a). Hydrophobic interactions have been recognized as a stabilizing factor in thermophilic proteins. Comparative studies have shown that 80 % of analyzed thermophilic proteins exhibit higher hydrophobicity than their mesophilic counterparts (Berezovsky et al., 2007; Gromiha et al., 2013).

Atomic temperature factors derived from the crystallographic data indicate the flexibility of different parts of the protein molecule (Fig. S7b). The most stable part of LysTt72 is the central β-sheet of the catalytic M23 domain (β1–β9), followed by the helix bundle α1–α5, especially α5, and some axial elements connecting the two structural domains. On the other hand, several surface loops display relatively high mobility, including loops surrounding the β-sheet and those flanking the middle part of the molecule. The flexible regions may act as "shock absorbers," allowing other parts of the protein to retain their structural integrity.

The evolution of viruses is subject to fewer constraints and proceeds at a faster rate than in cellular organisms. This enables a more rapid exploration of structural possibilities. Perhaps the unusual fold of LysTt72 is the result of such a deep foray into potential solutions to the problem of thermostability—solutions that would not be readily accessible to organisms less tolerant of mutations and evolving at a slower rate. The familiar M23 peptidase fold accounts for one-third of the protein structure, while the remaining two-thirds, which extend from the catalytic domain, have not been described previously (Fig. 5a and b). The uniqueness of this structure is further confirmed by amino acid sequence similarity searches, which identified only two other proteins likely to share a similar overall structure with LysTt72: two closely related uncharacterized endolysins—LysTMA from phage φTMA and LysYS40 from phage φYS40. Most differences between the three sequences can be mapped onto the surface of the molecule (Fig. S7c), consistent with the general observation that mutations are more easily tolerated on the protein surface than in its core. It is notable that the AlphaFold algorithm not only accurately modeled the familiar M23 domain, but also predicted the complete structure with remarkable precision (Fig. S4), including the regions for which no recognizable structural patterns were found (Fig. S8).

The unexpected electron density in the substrate-binding groove and at the active site indicates an affinity of the protein for ligands present in

its environment during the protein purification and crystallization (Fig. 5c). Peptides typical of *T. thermophilus* murein were absent in the *E. coli* expression system; instead, the protein picked up a component of the *E. coli* peptidoglycan from the solution. This is not surprising given that the enzymatic tests, described above, showed significant activity of LysTt72 against *E. coli* and other mesophilic bacteria.

The presence of ligands in the crystal structure presents an opportunity to consider the reaction mechanism and substrate specificity. The phosphate (or sulfate) bound at the active site could resemble the tetrahedral reaction intermediate. A bound tetrahedral anion has also been observed in LytM, another enzyme of the M23 family (Firczuk et al., 2005). However, in LytM, the anion was bound to Zn^{2+} in an asymmetric unidentate manner (making Zn^{2+} tetracoordinated), while another O atom of the ligand was positioned symmetrically between two His residues (His260 and His291), identified as essential for catalysis (Spencer et al., 2010). The protonated O atom of the anion donates H-bonds to the deprotonated N^{ε} and N^{δ} atoms of the His residues. In contrast to LytM, the anion bound to LysTt72 forms a symmetric bidentate interaction with Zn^{2+} (making Zn^{2+} pentacoordinated). The interaction of the anion with two equivalently placed His residues (His176 and His206) is also different. Two O atoms in the anion interact one-to-one with the two His residues. His176 is an H-bond acceptor from the phosphate (deprotonation of N^{ε} can be inferred because N^{δ} is positioned to donate an H-bond to the carbonyl O atom of Cys155). The protonation state of His206 cannot be inferred because its N^{δ} interacts with the hydroxyl group of Tyr204, which could act as either a donor or an acceptor.

The orientation and proximity of the bound peptide to the active site are also noteworthy. The electron density starts at the amino group of γ-D-Glu, and the residue expected to precede it, L-Ala, cannot be traced. L-Ala is either absent or disordered, and no attempt has been made to model it. However, the electron density ends approximately 5 Å from the Zn^{2+} cation, and the amino group is at H-bonding distance to the phosphate occupying the active site (Fig. 6). This finding is consistent with the expectation that peptides bind productively, as substrates, to the enzyme. The traceable electron density of the bound peptide includes γ-D-Glu (some disorder at its free carboxyl group), m-A2pm and L-Lys (both with clear density), and the main chain of the next residue, L-Arg. This sequence from *E. coli* murein can be compared to the expected sequence of the natural substrate from *T. thermophilus* peptidoglycan. L-Ala and γ-D-Glu are also found in *T. thermophilus*, but the next expected residue is L-ornithine. The side chain of m-A2pm has an amino group similar to that of ornithine but the side chain is longer by one $–CH_2–$ group and includes an additional carboxyl group. However, the substrate-binding groove appears to place no steric restrictions on the side chain as it points toward the solvent. Further away from the active site, the substrate-binding groove opens up even wider to accommodate additional residues (Fig. 5c).

In summary, this report identifies endopeptidase LysTt72 as a promising model for structural and functional studies to develop potent lysins to combat antibiotic-resistant bacterial pathogens. The protein's unique structural features are likely responsible for its thermostability. The interlaced extensions emerging from the catalytic domain—constituting most of the protein's structure—may represent a novel mechanism for enhancing thermostability. The structure adds to our understanding of thermostable proteins and offers new insight for protein engineering strategies to design thermostable and effective antimicrobial agents.

5. Methods

5.1. Bacterial strains, plasmids, phages and growth conditions

The vB_Tt72 phage and the host strain, *Thermus thermophilus* MAT72, were isolated from the hot spring in the Badstofuhver area in Hveragerdi, Iceland, and obtained from the MATIS collection of microorganisms, Iceland. *T. thermophilus* MAT72 cells were grown at 60 °C in TM medium containing, per liter, 4 g peptone, 2 g yeast extract, pH 7.2 [both from Difco Laboratories], 1 g NaCl, and 10 ml Castenholtz basal salts solution, pH 7.2 (Plotka et al., 2014). *Escherichia coli* strains DH5α and Rosetta 2(DE3) were used for molecular cloning and protein overproduction, respectively. The bacterial strains used as substrates for LysTt72 were obtained from the American Type Culture Collection (*Bacillus megaterium* ATCC 14581, *Deinococcus radiodurans* ATCC 13939), the Collection of Plasmids and Microorganisms KPD, University of Gdansk, Poland (*Acinetobacter baumannii* KPD 205-BA, *Bacillus subtilis* KPD 10, *Escherichia coli* MG1655 KPD 26-BA, *Listeria monocytogenes* KPD 1326, *Pseudomonas aeruginosa* KPD 124, *Salmonella* serovar *Panama* KPD 101-BA, *Serratia marcescens* KPD 102-BA, *Staphylococcus aureus* KPD 19), the Deutsche Sammlung von Mikroorganismen und Zellkulturen GmbH (*Thermus thermophilus* HB8 DSM 579, *Thermus thermophilus* HB27 DSM 7039, *Thermus parvatiensis* DSM 21745) and the MATIS collection of microorganisms (*Thermus scotoductus* MAT2631, *Thermus flavus* MAT1087). Mesophilic bacteria were cultivated at 37 °C in Luria broth (LB), whereas bacteria from the genus *Thermus* were grown at 60 °C in TM medium (Plotka et al., 2014). LB medium was supplemented with 100 μg/mL ampicillin and 34 μg/mL chloramphenicol when necessary. The plasmid pET15b (Novagen) was used for cloning and gene expression. The pET15b_LysTt72 plasmid constructed in this work was deposited in the Collection of Plasmids and Microorganisms at the University of Gdansk, Gdansk, Poland.

5.2. Gene cloning, overproduction and purification of the recombinant protein LysTt72

The *lysTt72* gene was amplified by PCR with gene-specific primers and phage vB_Tt72 DNA as a template (forward: 5′-CGAATTCCATATGGAACAGAAAGTTTACTTTCCG-3′ and reverse: 5′-CGCGGATCCTTATTGCACAGCGAAACAAATTTTC-3′). The respective primers were designed with NdeI and BamHI restriction sites (underlined). The PCR-amplified DNA fragment was digested with NdeI and BamHI restriction enzymes and ligated into the expression vector, pET15b linearized with the same enzymes. The ligation mixture was then transformed into *E. coli* DH5α cells. Positive transformants carrying pET15b_LysTt72 were selected using restriction enzyme digestion, and the clones were confirmed by DNA sequencing. *E. coli* Rosetta 2(DE3) cells with pET15b_LysTt72 were cultivated at 37 °C in LB medium supplemented with ampicillin and chloramphenicol. When the turbidity at 600 nm reached 0.5, isopropyl-β-D-thiogalactopyranoside (IPTG) was added to the culture to a final concentration of 1 mM. The cells were further cultured at 37 °C for 4 h. The cells were harvested by centrifugation (10 000 × g, 20 min, 4 °C) and stored at −80 °C for further use. The pelleted cells (4 g) were thawed and suspended in 5 mL of buffer A (50 mM sodium phosphate buffer, pH 8.0, 500 mM NaCl, 0.1 % [v/v] Triton X-100, 5 % [v/v] glycerol) with 10 mM imidazole. The suspension was sonicated for 6 min (sequences of 10 s pulse, 1 min pause). Next, the lysate was centrifuged (18 000 × g, 20 min, 4 °C), the pellet was discarded, and the supernatant was loaded into a 1 mL TALON® Metal Affinity Resin (Takara Bio) preequilibrated column. The column was washed with 15 mL of buffer A supplemented with 10 mM imidazole. The recombinant protein was eluted in buffer A with 200 mM imidazole. Fractions with the most protein were dialyzed in 20 mM HEPES (pH 7.4), 50 mM NaCl, and 50 % [v/v] glycerol and then stored at −20 °C. The protein concentration was determined by the Bradford assay (Bradford, 1976). The purity of the LysTt72 preparation was determined by SDS-PAGE (Fig. S2).

5.3. Size-exclusion chromatography

Size exclusion chromatography (SEC) analysis was performed using a Superdex 75 10/300 GL column (GE Healthcare) on an ÄKTA™ pure 25 chromatography system (GE Healthcare, USA). A LysTt72 (0.5 mg)

sample was loaded on a column equilibrated with 50 mM potassium phosphate buffer (pH 7.0) and 150 mM NaCl and eluted at a flow rate of 0.5 mL/min in the same buffer. The absorbance was measured at 280 nm (mAU, milli-absorbance units). The column was calibrated with proteins of known molecular masses: alcohol dehydrogenase (tetramer), 146.8 kDa; bovine serum albumin, 66 kDa; ovalbumin, 43 kDa; trypsin inhibitor, 22 kDa; and cytochrome *C*, 12.4 kDa (Sigma-Aldrich).

5.4. Turbidity reduction assays

The lytic activity of the LysTt72 was assessed using turbidity reduction assay (TRA) as previously described (Plotka et al., 2015). Chloroform-treated *T. thermophilus* MAT72 cells were used as the substrate. Briefly, *T. thermophilus* MAT72 cells (OD_{600} = 0.5) were collected by centrifugation and resuspended in chloroform-saturated 50 mM Tris-HCl, pH 7.7. The suspension was gently shaken for 45 min at room temperature. The cells were then washed with 10 mM potassium phosphate buffer, pH 8.0 (buffer B), to remove residual chloroform and were stored at −80 °C. The assay was conducted in a 96-well plate, with each reaction mixture containing 190 µL of chloroform-treated *T. thermophilus* MAT72 cells in buffer B (OD_{600} = 0.8–1.0) and 10-µL of enzyme at a concentrations of 50 µg/mL. The reaction was incubated for 60 min at 60 °C, and the decrease in the OD_{600} was measured over time using an EnSpire multimode plate reader (PerkinElmer, USA). Gram-negative bacteria were prepared essentially as described for *T. thermophilus* MAT72 cells. Gram-positive bacteria were collected by centrifugation during the late exponential to early stationary phase of growth. In each case, the cell pellet was washed and suspended in buffer B.

To determine the LysTt72 optimum the activity of the enzyme was assayed under various conditions. The variable factors were: (i) temperature (20–90 °C), (ii) pH range (5–11), and (iii) KCl concentration (0 to 750 mM). Chloroform-treated *T. thermophilus* MAT72 cells (OD_{600} = 1.0) were used for TRA assay as described above. The buffer with optimal pH and KCl concentration (20 mM Tris-HCl pH 9.5 and 25 mM KCl) was used for temperature optimization. Control reactions included reaction buffer in place of the enzyme aliquot. The lytic activity of LysTt72 under specific conditions was calculated as follows: OD_{600} (buffer only) − OD_{600} sample with endolysin)/initial OD600, as previously described (Plotka et al., 2015). All assays were repeated in triplicate.

5.5. Thermostability and thermoaggregation

Thermal stability and protein aggregation were analyzed by nano differential scanning fluorimetry (nanoDSF) and backreflection technology. Protein stability and aggregation tests were conducted simultaneously using a Prometheus NT.48 (NanoTemper Technologies, Germany). Standard-grade glass capillaries (NanoTemper Technologies) were filled with 10 µL of LysTt72 solution (1 mg/mL in 20 mM HEPES, pH 7.4, 50 mM NaCl and 5 % glycerol [v/v]) and placed into the sample holder. The temperature was gradually increased from 20 to 110 °C at a rate of 1 °C/min. Prior to measurement, samples were centrifuged for 10 min at 10 000 × g at 4 °C. Protein unfolding was monitored by detecting changes in Trp and Tyr fluorescence at emission wavelengths of 330 and 350 nm. Simultaneously, aggregation was tracked through intrinsic fluorescence. Data analysis was performed using PR.StabilityAnalysis software (NanoTemper Technologies). Melting temperatures (T_m), onset temperatures (T_{onset}) and mid-aggregation temperatures (T_{aag}) were calculated according to the manufacturer's instructions. All measurements were performed in triplicate.

5.6. Transmission electron microscopy

Transmission electron microscopy was performed as previously described (Szadkowska et al., 2024). Briefly, *T. thermophilus* MAT72 was grown in 20 mL of TM medium at 60 °C until reaching the exponential phase (OD_{600} = 0.45–0.5). The cells were then centrifuged (4 000 × g, 20 min, 4 °C), washed, and resuspended in 20 mM HEPES, pH 7.4, to a final titer of approx. 10^7 CFU/ mL. The bacteria were incubated at 55 °C for 2 h with LysTt72 (100 µg/mL). The control reaction included the reaction buffer in place of the enzyme. After incubation, the bacteria were pelleted again by centrifugation (4 000 × g, 20 min, 4 °C), washed twice with PBS (10 mM phosphate buffer, pH 7.4, 137 mM Nacl and 2.7 mM KCl), and the pellet was fixed with 2.5 % glutaraldehyde, followed by post-fixation with 1 % osmium tetroxide (Polysciences Inc., USA). After dehydration with ethanol, the bacteria were embedded in Epon 812 resin (Sigma-Aldrich, USA). Ultrathin sections (60 nm) were cut using an ultramicrotome (Leica UC7) and counterstained with lead citrate and uranyl acetate (Sigma-Aldrich, USA). The bacterial cell morphology was analyzed with a Tecnai Spirit BioTwin electron microscope (FEI Company, USA). TEM experiments were conducted at the Laboratory of Electron Microscopy (Faculty of Biology, University of Gdansk, Poland).

5.7. Protein crystallization, data collection, processing, structure solution and refinement

Prior to crystallization, LysTt72 was dialyzed into a buffer containing 50 mM NaCl and 25 mM HEPES, pH 8.0. The protein was crystallized using the crystallization screen Morpheus I (Molecular Dimensions). The following conditions were used: 20 % v/v PEG (polyehtylene glycol) 500 MME, 10 % w/v PEG 20000, 30 mM sodium nitrate, 30 mM sodium phosphate dibasic, 30 mM ammonium sulfate and 0.1 M 6.5 imidazole/ MES monohydrate (acid) at pH 6.5. The synchrotron X-ray diffraction data were collected at 100 K at beamline P13, operated by EMBL Hamburg at the PETRA storage ring (DESY, Hamburg, Germany) (Cianci et al., 2017). The X-ray diffraction data were processed using the XDS program (Kabsch, 2010). Two additional crystals (LysTt72a and LysTt72b) were analyzed over the next few months. The X-ray data are summarized in Table 2. The structure was solved by molecular replacement using Phaser (McCoy et al., 2007) from the CCP4 program suite (Winn et al., 2011). The starting model for molecular replacement was prepared based on a model predicted by AlphaFold (Jumper et al., 2021), by selecting the parts with a three-dimensional structure similar to that of peptidoglycan peptidase from *Campylobacter jejuni* (PDB ID 6JMY) (Min et al., 2020). The selected common parts shared 32 % sequence identity, and the model thus prepared represented approximately 40 % of LysTt72. Phaser was used to generate a single solution for the 2.2 Å LysTt72 X-ray data. The Z-score for the rotation function was 5.5 and for the translation function it was 6.9. The initial electron density map showed some features not included in the model, e.g. a bound ligand. The chemical structure of the ligand was drawn using the online Marvin JS sketcher (Chemaxon Ltd.). The chemical restraints for the ligand were calculated using Grade Web Server (Global Phasing Ltd). Iterative cycles of model building, with Coot (Emsley et al., 2010), and refinement with Refmac5 (Murshudov et al., 2011) resulted in a complete atomic model of the protein. The other two structures (LysTt72a and LysTt72b) were determined by molecular replacement using as the starting model the refined model of the first structure with water and other ligands removed, and subsequently, the models were refined like the first structure. The refinement is summarized in Table 2. The anomalous density maps were calculated using the anomalous amplitudes of the reflections, $|F^+-F^-|$, as Fourier coefficients and phases calculated from the refined atomic coordinates and retarded by 90°.

5.8. Phylogenetic analysis

Viral M23 peptidase protein sequences were retrieved from the UniProt database using the search query "(xref:pfam-PF01551) AND (taxonomy_id:10239)". Domain composition analysis was performed using the pfam_scan.pl script (obtained from ftp.ebi.ac.uk/pub/databa

Table 2
Summary of X-ray data and model refinement.

Crystal	LysTt72	LysTt72a	LysTt72b
PDB ID	8S3M	8S3U	8S3W
Space group	$P2_12_12_1$	$P2_12_12_1$	$P2_12_12_1$
Unit cell parameters			
a (Å)	44.13	40.53	44.37
b (Å)	60.99	60.15	61.02
c (Å)	125.34	124.25	124.98
α (°)	90	90	90
β (°)	90	90	90
γ (°)	90	90	90
Wavelength (Å)	0.7749	0.9790	0.9790
Beamline	EMBL P13	EMBL P13	EMBL P13
Temperature (K)	100	100	100
Resolution (Å)	2.2	2.3	2.5
R_{merge} [#]	0.128 (0.863)[*]	0.107 (1.65)	0.186 (2.03)
Completeness (%)	99.2	99.9	99.8
No. of reflections (unique)	87 943 (17 711)	184 296 (14 096)	162,037 (12 288)
<I/σ(I)>	8.71 (1.9)	13.6 (1.4)	9.9 (1.3)
R[§] / R_{free}[$]	0.187/0.260	0.193/0.298	0.186/0.281
No. atoms protein/ligand/ solvent/metal	2796/41/75/1	2796/41/31/1	2796/41/50/1
Av. B-factors: prot./lig./ solv./met. ($Å^2$)	42.5/63.8/ 40.1/26.6	74.1/96.8/ 63.2/49.0	64.9/83.7/ 56.7/48.8
R.m.s.d. from target values for bond lengths/ angles (Å,°)	0.007/1.6	0.009/1.9	0.007/1.7
Ramachandran % most favored/ additional allowed/ generously allowed/ disallowed	85.5/13.5/0.6/ 0.3	83.5/14.5/1.0/ 1.0	84.2/14.5/ 0.6/0.6
Raw diffraction images DOI	https://doi.org/10.18150/2W87AF	https://doi.org/10.18150/9TCUV8	https://doi.org/10.18150/IPEQFH

[*] Values in brackets are for the highest resolution shell.
[#] $R_{merge} = \Sigma_{hkl}\Sigma_i|I_i(hkl) - <I(hkl)>|/\Sigma_{hkl}\Sigma_i I_i(hkl)$, where $I_i(hkl)$ is the integrated intensity of a given reflection and $< I(hkl) >$ is the mean intensity of multiple corresponding symmetry-related reflections.
[§] $R = \Sigma_{hkl}||F_{obs}| - |F_{calc}||/\Sigma_{hkl}|F_{obs}|$, where F_{obs} and F_{calc} are the observed and calculated structure factors, respectively.
[$] R_{free} is R calculated using a randomly chosen subset of reflections excluded from the refinement.

ses/Pfam/Tools/) to identify Pfam domains. Sequences containing additional domains beyond the Peptidase family M23 (PF01551) were excluded from subsequent analysis. To reduce redundancy in the dataset, sequences were clustered using the MMseqs2 easy-cluster workflow with sequence identity and coverage thresholds set to 70 % (Steinegger and Söding, 2017). Representative sequences from each cluster were selected for phylogenetic analysis. Multiple sequence alignment was performed using MUSCLE v5.1 with the −super5 flag (Edgar, 2022). The resulting alignment was refined using ClipKit v2.3.0 in smart-gap mode to remove poorly aligned regions (Steenwyk et al., 2020). Phylogenetic tree construction was performed using IQ-TREE2 v2.3.6 with model selection and 2000 ultrafast bootstrap iterations (Minh et al., 2020). The resulting phylogenetic tree was visualized using the Interactive Tree of Life (iTOL) web server v6 and later manually annotated (Letunic and Bork, 2024). For the structure-guided tree the structures for all above mentioned sequences included in the phylogenetic tree have been predicted using AlphaFold3 (Abramson et al., 2024) and then aligned using FoldMason (Gilchrist et al., 2024). Next, a maximum-likelihood tree was constructed using IQ-tree2, same as with the phylogenetic tree.

CRediT authorship contribution statement

Sebastian Dorawa: Writing – original draft, Visualization, Methodology, Investigation, Formal analysis, Data curation, Conceptualization. **Katarzyna Biniek-Antosiak:** Investigation, Conceptualization. **Magdalena Bejger:** Investigation, Conceptualization. **Anna-Karina Kaczorowska:** Writing – review & editing, Validation, Methodology, Investigation, Formal analysis, Data curation, Conceptualization. **Karol Ciuchcinski:** Visualization, Software, Investigation, Formal analysis. **Agnieszka Godlewska:** Investigation. **Magdalena Płotka:** Methodology, Formal analysis. **Gudmundur O. Hreggvidsson:** Resources. **Lukasz Dziewit:** Validation, Software, Investigation, Formal analysis. **Tadeusz Kaczorowski:** Writing – review & editing, Writing – original draft, Validation, Supervision, Project administration, Methodology, Formal analysis, Conceptualization. **Wojciech Rypniewski:** Writing – review & editing, Writing – original draft, Visualization, Validation, Supervision, Investigation, Formal analysis, Conceptualization.

Declaration of competing interest

The authors declare that they have no known competing financial interests or personal relationships that could have appeared to influence the work reported in this paper.

Acknowledgments

This research was funded by the Norway Financial Mechanism through the National Science Centre (Poland) GRIEG1 grant: UMO-2019/34/H/NZ2/00584. The authors thank Future Synthesis sp. z o.o. for support and reagents.

Appendix A. Supplementary data

Supplementary data to this article can be found online at https://doi.org/10.1016/j.jsb.2025.108230.

Data availability

The nucleotide and protein sequences of LysTt72 were deposited in GenBank under the accession number PQ465150. The raw X-ray diffraction images were deposited in the Macrocrystallographic Xtallography Raw Data Repository (MX-RDR) and are available under the DOI addresses given in Table 2. The refined atomic coordinates of the LysTt72 models were deposited in the Protein Data Bank (PDB) under the IDs listed in Table 2.

References

Abdelrahman, F., Easwaran, M., Daramola, O.I., Ragab, S., Lynch, S., Oduselu, T.J., Khan, F.M., Ayobami, A., Adnan, F., Torrents, E., Sanmukh, S., El-Shibiny, A., 2021. Phage-Encoded Endolysins. Antibiotics (basel) 10, 124. https://doi.org/10.3390/antibiotics10020124.

Abramson, J., Adler, J., Dunger, J., Evans, R., Green, T., Pritzel, A., Ronneberger, O., Willmore, L., Ballard, A.J., Bambrick, J., Bodenstein, S.W., Evans, D.A., Hung, C.-C., O'Neill, M., Reiman, D., Tunyasuvunakool, K., Wu, Z., Žemgulytė, A., Arvaniti, E., Beattie, C., Bertolli, O., Bridgland, A., Cherepanov, A., Congreve, M., Cowen-Rivers, A.I., Cowie, A., Figurnov, M., Fuchs, F.B., Gladman, H., Jain, R., Khan, Y.A., Low, C.M.R., Perlin, K., Potapenko, A., Savy, P., Singh, S., Stecula, A., Thillaisundaram, A., Tong, C., Yakneen, S., Zhong, E.D., Zielinski, M., Žídek, A., Bapst, V., Kohli, P., Jaderberg, M., Hassabis, D., Jumper, J.M., 2024. Accurate structure prediction of biomolecular interactions with AlphaFold 3. Nature 630, 493–500. https://doi.org/10.1038/s41586-024-07487-w.

Acosta, F., Alvarez, L., de Pedro, M.A., Berenguer, J., 2012a. Localized synthesis of the outer envelope from Thermus thermophilus. Extremophiles 16, 267–275. https://doi.org/10.1007/s00792-011-0427-7.

Acosta, F., Ferreras, E., Berenguer, J., 2012b. The β-barrel assembly machinery (BAM) is required for the assembly of a primitive S-layer protein in the ancient outer membrane of Thermus thermophilus. Extremophiles: Life under Extreme Conditions 16. https://doi.org/10.1007/s00792-012-0480-x.

A. Aevarsson, A.-K. Kaczorowska, B.T. Adalsteinsson, J. Ahlqvist, S. Al-Karadaghi, J. Altenbuchner, H. Arsin, Ú.Á. Átlasson, D. Brandt, M. Cichowicz-Cieślak, K.A.S. Cornish, J. Courtin, S. Dabrowski, H. Dahle, S. Djeffane, S. Dorawa, J. Dusaucy, F. Enault, A.-E. Fedøy, S. Freitag-Pohl, O.H. Fridjonsson, C. Galiez, E. Glomsaker, M. Guérin, S.E. Gundesø, E.E. Gudmundsdóttir, H. Gudmundsson, M. Håkansson, C. Henke, A. Helleux, J.R. Henriksen, S. Hjörleifdóttir, G.O. Hreggvidsson, A. Jasilionis, A. Jochheim, I. Jónsdóttir, L.B. Jónsdóttir, A. Jurczak-Kurek, T. Kaczorowski, J. Kalinowski, L.P. Kozlowski, M. Krupovic, K. Kwiatkowska-Semrau, O. Lanes, J. Lange, J. Lebrat, J. Linares-Pastén, Y. Liu, S.A. Lorentsen, T. Lutterman, T. Mas, W. Merré, M. Mirdita, A. Morzywołek, E.O. Ndela, E.N. Karlsson, E. Olgudóttir, C.

Pedersen, F. Perler, S.K. Pétursdóttir, M. Plotka, E. Pohl, D. Prangishvili, J.L. Ray, B. Reynisson, T. Róbertsdóttir, R.-A. Sandaa, A. Sczyrba, S. Skírnisdóttir, J. Söding, T. Solstad, I.H. Steen, S.K. Stefánsson, M. Steinegger, K.S. Overå, B. Striberny, A. Svensson, M. Szadkowska, E.J. Tarrant, P. Terzian, M. Tourigny, T. van den Bergh, J. Vanhalst, J. Vincent, B. Vroling, B. Walse, L. Wang, H. Watzlawick, M. Welin, O. Werbowy, E. Wons, R. Zhang, Going to extremes - a metagenomic journey into the dark matter of life, FEMS Microbiol Lett 368 (2021) fnab067. DOI: 10.1093/femsle/fnab067.

Berezovsky, I.N., Zeldovich, K.B., Shakhnovich, E.I., 2007. Positive and negative Design in Stability and Thermal Adaptation of Natural Proteins. PLoS Comput. Biol. 3, e52.

Bradford, M.M., 1976. A rapid and sensitive method for the quantitation of microgram quantities of protein utilizing the principle of protein-dye binding. Anal. Biochem. 72, 248–254. https://doi.org/10.1006/abio.1976.9999.

Briers, Y., Lavigne, R., 2015. Breaking barriers: expansion of the use of endolysins as novel antibacterials against Gram-negative bacteria. Future Microbiol. 10, 377–390. https://doi.org/10.2217/fmb.15.8.

Carugo, O., 2008. Amino acid composition and protein dimension. Protein Sci. 17, 2187–2191. https://doi.org/10.1110/ps.037762.108.

M. Cianci, G. Bourenkov, G. Pompidor, I. Karpics, J. Kallio, I. Bento, M. Roessle, F. Cipriani, S. Fiedler, T.R. Schneider, IUCr, P13, the EMBL macromolecular crystallography beamline at the low-emittance PETRA III ring for high- and low-energy phasing with variable beam focusing, Urn:Issn:1600-5775 24 (2017) 323–332. DOI: 10.1107/S1600577516016465.

Dams, D., Briers, Y., 2019. Enzybiotics: Enzyme-based Antibacterials as Therapeutics. Adv. Exp. Med. Biol. 1148, 233–253. https://doi.org/10.1007/978-981-13-7709-9_11.

De Oliveira, D.M.P., Forde, B.M., Kidd, T.J., Harris, P.N.A., Schembri, M.A., Beatson, S. A., Paterson, D.L., Walker, M.J., 2020. Antimicrobial Resistance in ESKAPE Pathogens. Clin. Microbiol. Rev. 33, e00181–e00219. https://doi.org/10.1128/CMR.00181-19.

Dziarski, R., Gupta, D., 2010. Review: Mammalian peptidoglycan recognition proteins (PGRPs) in innate immunity. Innate Immun. 16, 168–174. https://doi.org/10.1177/1753425910366059.

Edgar, R.C., 2022. Muscle5: High-accuracy alignment ensembles enable unbiased assessments of sequence homology and phylogeny. Nat. Commun. 13, 6968. https://doi.org/10.1038/s41467-022-34630-w.

Emsley, P., Lohkamp, B., Scott, W.G., Cowtan, K., 2010. Features and development of Coot, Acta Crystallographica. Section D, Biological Crystallography 66, 486–501. https://doi.org/10.1107/S0907444910007493.

Farias, S.T., Bonato, M.C.M., 2003. Preferred amino acids and thermostability. Genet. Mol. Res. 2, 383–393.

Firczuk, M., Mucha, A., Bochtler, M., 2005. Crystal structures of active LytM. J. Mol. Biol. 354, 578–590. https://doi.org/10.1016/j.jmb.2005.09.082.

Gerstmans, H., Grimon, D., Gutiérrez, D., Lood, C., Rodríguez, A., van Noort, V., Lammertyn, J., Lavigne, R., Briers, Y., 2020. A VersaTile-driven platform for rapid hit-to-lead development of engineered lysins. Sci Adv 6, eaaz1136. https://doi.org/10.1126/sciadv.aaz1136.

C.L.M. Gilchrist, M. Mirdita, M. Steinegger, Multiple Protein Structure Alignment at Scale with FoldMason, (2024) 2024.08.01.606130. DOI: 10.1101/2024.08.01.606130.

Grabowska, M., Jagielska, E., Czapinska, H., Bochtler, M., Sabala, I., 2015. High resolution structure of an M23 peptidase with a substrate analogue. Sci. Rep. 5, 14833. https://doi.org/10.1038/srep14833.

Gromiha, M.M., Pathak, M.C., Saraboji, K., Ortlund, E.A., Gaucher, E.A., 2013. Hydrophobic environment is a key factor for the stability of thermophilic proteins. Proteins 81, 715–721. https://doi.org/10.1002/prot.24232.

Grote, A., Hiller, K., Scheer, M., Münch, R., Nörtemann, B., Hempel, D.C., Jahn, D., 2005. JCat: a novel tool to adapt codon usage of a target gene to its potential expression host. Nucleic Acids Res. 33, W526–W531. https://doi.org/10.1093/nar/gki376.

Henne, A., Bruggemann, H., Raasch, C., Wiezer, A., Hartsch, T., Liesegang, H., Johann, A., Lienard, T., Gohl, O., Martinez-Arias, R., Jacobi, C., Starkuviene, V., Schlenczeck, S., Dencker, S., Huber, R., Klenk, H.-P., Kramer, W., Merkl, R., Gottschalk, G., Fritz, H.-J., 2004. The genome sequence of the extreme thermophile Thermus thermophilus. Nat. Biotechnol. 22, 547–554.

Holm, L., 2020. DALI and the persistence of protein shape. Protein Sci. 29, 128–140. https://doi.org/10.1002/PRO.3749.

Ikai, A., 1980. Thermostability and aliphatic index of globular proteins. The Journal of Biochemistry 88, 1895–1898. https://doi.org/10.1093/oxfordjournals.jbchem.a133168.

Jumper, J., Evans, R., Pritzel, A., Green, T., Figurnov, M., Ronneberger, O., Tunyasuvunakool, K., Bates, R., Žídek, A., Potapenko, A., Bridgland, A., Meyer, C., Kohl, S.A.A., Ballard, A.J., Cowie, A., Romera-Paredes, B., Nikolov, S., Jain, R., Adler, J., Back, T., Petersen, S., Reiman, D., Clancy, E., Zielinski, M., Steinegger, M., Pacholska, M., Berghammer, T., Bodenstein, S., Silver, D., Vinyals, O., Senior, A.W., Kavukcuoglu, K., Kohli, P., Hassabis, D., 2021. Highly accurate protein structure prediction with AlphaFold. Nature 596, 583–589. https://doi.org/10.1038/s41586-021-03819-2.

Kabsch, W., 2010. XDS. Acta Crystallogr. D Biol. Crystallogr. 66, 125. https://doi.org/10.1107/S0907444909047337.

Kim, S.J., Chang, J., Singh, M., 1848. Peptidoglycan architecture of Gram-positive bacteria by solid-state NMR. Biochim. Biophys. Acta 2015, 350–362. https://doi.org/10.1016/j.bbamem.2014.05.031.

Kumar, S., Tsai, C.-J., Nussinov, R., 2000. Factors enhancing protein thermostability. Protein Eng. Des. Sel. 13, 179–191. https://doi.org/10.1093/protein/13.3.179.

Letunic, I., Bork, P., 2024. Interactive tree of Life (iTOL) v6: recent updates to the phylogenetic tree display and annotation tool. Nucleic Acids Res. 52, W78–W82. https://doi.org/10.1093/nar/gkae268.

Loessner, M.J., 2005. Bacteriophage endolysins–current state of research and applications. Curr. Opin. Microbiol. 8, 480–487. https://doi.org/10.1016/j.mib.2005.06.002.

Ma, B.-G., Song, Q.-S., Zhang, H.-Y., 2006. CvP-bias as an index to predict the life style of last common ancestor. J. Biomol. Struct. Dyn. 23, 555–558. https://doi.org/10.1080/07391102.2006.10507080.

McCoy, A.J., Grosse-Kunstleve, R.W., Adams, P.D., Winn, M.D., Storoni, L.C., Read, R.J., 2007. Phaser crystallographic software. J. Appl. Cryst. 40, 658–674. https://doi.org/10.1107/S0021889807021206.

Min, K., An, D.R., Yoon, H.-J., Rana, N., Park, J.S., Kim, J., Lee, M., Hesek, D., Ryu, S., Kim, B.M., Mobashery, S., Suh, S.W., Lee, H.H., 2020. Peptidoglycan reshaping by a noncanonical peptidase for helical cell shape in campylobacter jejuni. Nat. Commun. 11, 458. https://doi.org/10.1038/s41467-019-13934-4.

Minh, B.Q., Schmidt, H.A., Chernomor, O., Schrempf, D., Woodhams, M.D., von Haeseler, A., Lanfear, R., 2020. IQ-TREE 2: New models and efficient methods for phylogenetic inference in the genomic era. Mol. Biol. Evol. 37, 1530–1534. https://doi.org/10.1093/molbev/msaa015.

Murshudov, G.N., Skubák, P., Lebedev, A.A., Pannu, N.S., Steiner, R.A., Nicholls, R.A., Winn, M.D., Long, F., Vagin, A.A., 2011. REFMAC5 for the refinement of macromolecular crystal structures. Acta Crystallogr. D Biol. Crystallogr. 67, 355. https://doi.org/10.1107/S0907444911001314.

Naryshkina, T., Liu, J., Florens, L., Swanson, S.K., Pavlov, A.R., Pavlova, N.V., Inman, R., Minakhin, L., Kozyavkin, S.A., Washburn, M., Mushegian, A., Severinov, K., 2006. Thermus thermophilus bacteriophage phiYS40 genome and proteomic characterization of virions. J. Mol. Biol. 364, 667–677. https://doi.org/10.1016/j.jmb.2006.08.087.

Oliveira, H., São-José, C., Azeredo, J., 2018. Phage-Derived Peptidoglycan Degrading Enzymes: challenges and Future prospects for In Vivo Therapy. Viruses 10, 292. https://doi.org/10.3390/v10060292.

Oshima, T., Imahori, K., 1974. Description of Thermus thermophilus (Yoshida and Oshima) comb. nov., a Nonsporulating Thermophilic Bacterium from a Japanese thermal Spa. Int. J. Syst. Evol. Microbiol. 24, 102–112. https://doi.org/10.1099/00207713-24-1-102.

Plotka, M., Kaczorowska, A.-K., Stefanska, A., Morzywolek, A., Fridjonsson, O.H., Dunin-Horkawicz, S., Kozlowski, L., Hreggvidsson, G.O., Kristjansson, J.K., Dabrowski, S., Bujnicki, J.M., Kaczorowski, T., 2014. Novel Highly Thermostable Endolysin from Thermus scotoductus MAT2119 Bacteriophage Ph2119 with Amino Acid Sequence Similarity to Eukaryotic Peptidoglycan Recognition Proteins. Appl. Environ. Microbiol. 80, 886–895. https://doi.org/10.1128/AEM.03074-13.

Plotka, M., Kaczorowska, A.-K., Morzywolek, A., Makowska, J., Kozlowski, L.P., Thorisdottir, A., Skírnisdottir, S., Hjörleifsdottir, S., Fridjonsson, O.H., Hreggvidsson, G.O., Kristjansson, J.K., Dabrowski, S., Bujnicki, J.M., Kaczorowski, T., 2015. Biochemical Characterization and Validation of a Catalytic Site of a Highly Thermostable Ts2631 Endolysin from the Thermus scotoductus Phage vb_tsc2631. PLoS One 10, e0137374. https://doi.org/10.1371/journal.pone.0137374.

Plotka, M., Kapusta, M., Dorawa, S., Kaczorowska, A.-K., Kaczorowski, T., 2019a. Ts2631 Endolysin from the Extremophilic Thermus scotoductus Bacteriophage vb_tsc2631 as an Antimicrobial Agent against Gram-negative Multidrug-Resistant Bacteria. Viruses 11, 657. https://doi.org/10.3390/v11070657.

Plotka, M., Sancho-Vaello, E., Dorawa, S., Kaczorowska, A.-K., Kozlowski, L.P., Kaczorowski, T., Zeth, K., 2019b. Structure and function of the Ts2631 endolysin of Thermus scotoductus phage vb_tsc2631 with unique N-terminal extension used for peptidoglycan binding. Sci. Rep. 9, 1261. https://doi.org/10.1038/s41598-018-37417-6.

Plotka, M., Szadkowska, M., Håkansson, M., Kovačič, R., Al-Karadaghi, S., Walse, B., Werbowy, O., Kaczorowska, A.-K., Kaczorowski, T., 2020. Molecular Characterization of a Novel Lytic Enzyme LysC from Clostridium intestinale URNW and its Antibacterial activity Mediated by Positively Charged N-Terminal Extension. Int. J. Mol. Sci. 21, 4894. https://doi.org/10.3390/ijms21144894.

Qi, Y.-L., Chen, Y.-T., Xie, Y.-G., Li, Y.-X., Rao, Y.-Z., Li, M.-M., Xie, Q.-J., Cao, X.-R., Chen, L., Qu, Y.-N., Yuan, Z.-X., Xiao, Z.-C., Lu, L., Jiao, J.-Y., Shu, W.-S., Li, W.-J., Hedlund, B.P., Hua, Z.-S., 2024. Analysis of nearly 3000 archaeal genomes from terrestrial geothermal springs sheds light on interconnected biogeochemical processes. Nat. Commun. 15, 4066. https://doi.org/10.1038/s41467-024-48498-5.

Quintela, J.C., Caparrós, M., de Pedro, M.A., 1995. Variability of peptidoglycan structural parameters in gram-negative bacteria. FEMS Microbiol. Lett. 125, 95–100. https://doi.org/10.1111/j.1574-6968.1995.tb07341.x.

Quintela, J.C., Pittenauer, E., Allmaier, G., Arán, V., de Pedro, M.A., 1995. Structure of peptidoglycan from Thermus thermophilus HB8. J. Bacteriol. 177, 4947–4962.

Quintela, J.C., García-del Portillo, F., Pittenauer, E., Allmaier, G., de Pedro, M.A., 1999a. Peptidoglycan fine structure of the radiotolerant bacterium Deinococcus radiodurans Sark. J Bacteriol 181, 334–337. https://doi.org/10.1128/JB.181.1.334-337.1999.

Quintela, J.C., Zöllner, P., García-del Portillo, F., Allmaier, G., de Pedro, M.A., 1999b. Cell wall structural divergence among Thermus spp. FEMS Microbiol Lett 172 223–229. https://doi.org/10.1111/j.1574-6968.1999.tb13472.x.

Rawlings, N.D., Tolle, D.P., Barrett, A.J., 2004. MEROPS: the peptidase database. Nucleic Acids Res. 32, D160–D164. https://doi.org/10.1093/nar/gkh071.

Razew, A., Schwarz, J.-N., Mitkowski, P., Sabala, I., Kaus-Drobek, M., 2022. One fold, many functions—M23 family of peptidoglycan hydrolases. Front. Microbiol. 13, 1036964. https://doi.org/10.3389/fmicb.2022.1036964.

Royet, J., Gupta, D., Dziarski, R., 2011. Peptidoglycan recognition proteins: Modulators of the microbiome and inflammation. Nat. Rev. Immunol. 11, 837–851. https://doi.org/10.1038/nri3089.

São-José, C., Costa, A.R., Melo, L.D.R., 2022. Editorial: Bacteriophages and their lytic enzymes as alternative antibacterial therapies in the age of antibiotic resistance. Front. Microbiol. 13, 884176. https://doi.org/10.3389/fmicb.2022.884176.

Spencer, J., Murphy, L.M., Conners, R., Sessions, R.B., Gamblin, S.J., 2010. Crystal structure of the LasA virulence factor from Pseudomonas aeruginosa: substrate specificity and mechanism of M23 metallopeptidases. J. Mol. Biol. 396, 908–923. https://doi.org/10.1016/j.jmb.2009.12.021.

Steenwyk, J.L., Iii, T.J.B., Li, Y., Shen, X.-X., Rokas, A., 2020. ClipKIT: a multiple sequence alignment trimming software for accurate phylogenomic inference. PLoS Biol. 18, e3001007. https://doi.org/10.1371/journal.pbio.3001007.

Steinegger, M., Söding, J., 2017. MMseqs2 enables sensitive protein sequence searching for the analysis of massive data sets. Nat. Biotechnol. 35, 1026–1028. https://doi.org/10.1038/nbt.3988.

Suhre, K., Claverie, J.-M., 2003. Genomic correlates of hyperthermostability, an update. J. Biol. Chem. 278, 17198–17202. https://doi.org/10.1074/jbc.M301327200.

Szadkowska, M., Kocot, A.M., Sowik, D., Wyrzykowski, D., Jankowska, E., Kozlowski, L. P., Makowska, J., Plotka, M., 2024. Molecular characterization of the PhiKo endolysin from Thermus thermophilus HB27 bacteriophage phiKo and its cryptic lytic peptide RAP-29. Front. Microbiol. 14. https://doi.org/10.3389/fmicb.2023.1303794.

Tamakoshi, M., Murakami, A., Sugisawa, M., Tsuneizumi, K., Takeda, S., Saheki, T., Izumi, T., Akiba, T., Mitsuoka, K., Toh, H., Yamashita, A., Arisaka, F., Hattori, M., Oshima, T., Yamagishi, A., 2011. Genomic and proteomic characterization of the large Myoviridae bacteriophage ϕTMA of the extreme thermophile Thermus thermophilus. Bacteriophage 1, 152–164. https://doi.org/10.4161/bact.1.3.16712.

Taylor, T.J., Vaisman, I.I., 2010. Discrimination of thermophilic and mesophilic proteins. BMC Struct. Biol. 10, S5. https://doi.org/10.1186/1472-6807-10-S1-S5.

Thompson, J.D., Higgins, D.G., Gibson, T.J., 1994. CLUSTAL W: improving the sensitivity of progressive multiple sequence alignment through sequence weighting, position-specific gap penalties and weight matrix choice. Nucleic Acids Res. 22, 4673–4680. https://doi.org/10.1093/nar/22.22.4673.

Vollmer, W., Bertsche, U., 2008. Murein (peptidoglycan) structure, architecture and biosynthesis in Escherichia coli. Biochim. Biophys. Acta 1778, 1714–1734. https://doi.org/10.1016/j.bbamem.2007.06.007.

Vollmer, W., Blanot, D., de Pedro, M.A., 2008a. Peptidoglycan structure and architecture. FEMS Microbiol. Rev. 32, 149–167. https://doi.org/10.1111/j.1574-6976.2007.00094.x.

Vollmer, W., Joris, B., Charlier, P., Foster, S., 2008b. Bacterial peptidoglycan (murein) hydrolases. FEMS Microbiol. Rev. 32, 259–286. https://doi.org/10.1111/j.1574-6976.2007.00099.x.

Wang, J., Chitsaz, F., Derbyshire, M.K., Gonzales, N.R., Gwadz, M., Lu, S., Marchler, G. H., Song, J.S., Thanki, N., Yamashita, R.A., Yang, M., Zhang, D., Zheng, C., Lanczycki, C.J., Marchler-Bauer, A., 2023. The conserved domain database in 2023. Nucleic Acids Res. 51, D384–D388. https://doi.org/10.1093/nar/gkac1096.

Winn, M.D., Ballard, C.C., Cowtan, K.D., Dodson, E.J., Emsley, P., Evans, P.R., Keegan, R. M., Krissinel, E.B., Leslie, A.G.W., McCoy, A., McNicholas, S.J., Murshudov, G.N., Pannu, N.S., Potterton, E.A., Powell, H.R., Read, R.J., Vagin, A., Wilson, K.S., 2011. Overview of the CCP4 suite and current developments, Acta Crystallographica. Section D, Biological Crystallography 67, 235–242. https://doi.org/10.1107/S0907444910045749.

Young, R., 2014. Phage lysis: three steps, three choices, one outcome. J. Microbiol. 52, 243–258. https://doi.org/10.1007/s12275-014-4087-z.

Zeldovich, K.B., Berezovsky, I.N., Shakhnovich, E.I., 2007. Protein and DNA sequence determinants of thermophilic adaptation. PLoS Comput. Biol. 3, e5.

Zeng, T., Liu, S., Zou, P., Yao, X., Chen, Q., Wei, L., Wang, Q., Zhang, C., Zheng, Y., Yu, R., 2024. Create artilysins from a recombinant library to serve as bactericidal and antibiofilm agents targeting Pseudomonas aeruginosa. Int. J. Biol. Macromol. 273, 132990. https://doi.org/10.1016/j.ijbiomac.2024.132990.